

SCIENTIFIC REPORTS



OPEN

Microstructure formation and interface characteristics of directionally solidified TiAl-Si alloys in alumina crucibles with a new Y_2O_3 skull-aided technology

Received: 22 August 2016
Accepted: 22 February 2017
Published: 23 March 2017

Jianglei Fan¹, Jianxiu Liu¹, Shen Wu¹, Shuxia Tian¹, Hongxia Gao¹, Shengyong Wang¹, Jingjie Guo² & Xiao Wang³

The microstructure evolution and interface characteristics of a directionally solidified Ti-43Al-3Si (at.%) alloy in an alumina (Al_2O_3) crucible with new Y_2O_3 skull-aided technology were investigated. The Y_2O_3 -skull that is in contact with the TiAl-melt is relatively stable, which results in a more controlled reaction between the skull and the melt than in the case of an Al_2O_3 crucible is used. A thin reaction layer was formed between the mould and the melt through mutual diffusion. The layer thickness increased with increasing reaction time. The thickness of this layer was less than $80\ \mu m$ for reaction times up to 5800 s. Y_2O_3 particles were not found in the specimen because the mould coating was prepared with fine Y_2O_3 powder without a binder, which prevented the Y_2O_3 particles splitting from the coating as a consequence of thermal physical erosion. The oxygen content of the TiAl-alloy increased with increasing reaction time. The total oxygen content of the solidified specimen was less than that of the specimen solidified in the Al_2O_3 crucibles. This new Y_2O_3 skull-aided technology is expected to improve the surface quality of TiAl-alloys and reduce the reaction between the crucible/mould and molten TiAl alloys during directional solidification processing with longer contact times.

γ -TiAl-based alloys have numerous attractive properties: they are lightweight, resistant to oxidation and strong at high temperatures^{1–5}. These properties meet the demands of next-generation aircraft and automotive engines. The main obstacles that limit commercial applications of TiAl alloys are their inherently brittle nature, low fluidity and high processing cost⁶. Nevertheless, the casting process provides a method with advantages for the manufacture of TiAl alloys when compared to forging and rolling⁷. Various techniques have been applied to investigate the solidification behaviours of TiAl alloys, such as the optical floating zone method^{8,9}, Bridgman method^{10–14}, water-cooled copper crucible method^{15–19}, and electromagnetic confinement method^{20–22}. Because of the well-known high reactivity of the melt, the selection of the mould material for casting of TiAl alloys is important.

Until now, a reaction between the metal and crucible was inevitable and led to metal contamination^{23–26}. Hence, imparting the inner face of the mould with high chemical stability, mechanical stability, and thermal stability is a key factor for the precision casting of γ -TiAl alloys^{27,28}. In the case of TiAl alloys, the materials commonly used for crucibles or moulds are oxide ceramics such as Y_2O_3 ^{29,30}, CaO ³¹, Al_2O_3 ^{32–36}, ZrO_2 ^{37,38}, $CaZrO_3$ ³⁹, AlN ⁴⁰ or BN ⁴¹. The reaction between the TiAl alloy melt and crucible can be controlled over a relatively short solidification time using these materials^{33,42}. Nonetheless, with a longer contact time, the surface quality and microstructure of TiAl alloys are still difficult to effectively control. Some methods that do not include a container, such as optical and induction floating zone furnaces^{9,43–45} and the electromagnetic confinement method, are also

¹Institute of Mechanical and Electrical Engineering, Zhengzhou University of Light Industry, Zhengzhou, 450002, P. R. China. ²School of Material Science and Engineering, Harbin Institute of Technology, Harbin, 150001, P. R. China. ³School of Energy and Power Engineering, Zhengzhou University of Light Industry, Zhengzhou, 450002, P. R. China. Correspondence and requests for materials should be addressed to J.F. (email: JLFan2011@163.com) or J.L. (email: jianxiuliu@126.com)

used for fundamental directional solidification studies of TiAl alloys^{22,46}. From the perspective of cost, using oxide ceramic crucible/mould remains the best choice for preparing castings of TiAl alloys by Y_2O_3 is regarded as the best crucible material; however, Y_2O_3 is expensive and exhibits poor thermal shock resistance⁴⁷. Although CaO is more inert than Al_2O_3 , moisture accumulation hinders its practical applications³¹. Despite being less stable than Y_2O_3 and CaO, Al_2O_3 is still the best choice for casting TiAl alloys because of its good thermal shock resistance and lower cost⁴⁸. Therefore, Al_2O_3 is often used as the crucible materials for the directional solidification of TiAl alloys^{32–34,36}. Coatings are commonly applied to Al_2O_3 crucible in directional solidification experiments involving TiAl alloys⁴⁹. However, the contamination of Y_2O_3 particles by atmospheric oxygen during the long solidification process needs to be minimized.

The purpose of the present work is to investigate the microstructure formation and interface characteristics of directionally solidified Ti-43Al-3Si (at.%) alloys with a new Y_2O_3 skull-aided technology under different reaction times. These results will contribute to the surface quality control of investment casting and the directional solidification of TiAl-based alloys.

Results and Discussion

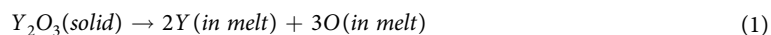
Microstructure formation. The structure of the directionally solidified Ti-43Al-3Si (at.%) alloy is shown in Fig. 1. The macrostructure of the specimen is shown in Fig. 1a. The specimen grew with columnar grains aligned along the drawing direction. The morphology of the solid-liquid interface was preserved by quenching and was cellular under the present solidification conditions. The macrostructures on the transverse sections are shown in Fig. 1b1–e1. These images indicate that the microstructure was uniform throughout the entire specimen. The microstructure of the Ti-43Al-3Si (at.%) alloy after directional solidification is a full-lamellar structure with silicide, as shown in Fig. 1b2–e2.

According to the XRD pattern shown in Fig. 2, the specimen consisted of TiAl, Ti_3Al and Ti_5Si_3 phases. Y_2O_3 particles were not found in the specimen, unlike the results of previous studies³⁰. This lack of Y_2O_3 particles is attributed to the coating of the mould being prepared using fine Y_2O_3 powder without a binder, resulting in fewer Y_2O_3 particles being split from the coating via thermal physical erosion. These observations indicate that the poor thermal shock resistance of the Y_2O_3 crucible could be improved using this method. Backscattered electron (BSE) mode scanning electron microscopy (SEM) images of the microstructures are shown in Fig. 3. A Composition analysis of the phases was conducted using energy-dispersive X-ray spectroscopy (EDX); the results are shown in Fig. 4. On the basis of the EDX results, the black, grey and white phases were identified as TiAl, Ti_3Al and Ti_5Si_3 phases, respectively.

Interface characteristics. The surface morphology of the solidified specimen is shown in Fig. 4. A reaction region with inclusions was not formed as described by Cui⁵⁰. Instead, a discontinuous bright layer with greater compactness on the surface was observed. As shown in Fig. 4, the bright layer consisted of Y, O, and areas of Al. Because the surface of the specimen was cleaned by ultrasonication before observation, the bright layer was a reaction layer between the Y_2O_3 skull and the TiAl melt rather than an adhesive layer of Y_2O_3 on the surface. The thickness of the reaction layer between the crucible and the melt increased with increasing reaction time, as shown in Fig. 5. The maximum thickness of the reaction layer was less than $15\ \mu\text{m}$, as shown in Fig. 5d. The severe reaction between the Al_2O_3 crucible and the melt for the directionally solidified specimen did not occur with a long reaction time (5800 s). This may be due to the high stability of Y_2O_3 in the TiAl melts diminishing the reaction between the mould and the TiAl melt.

Variations in composition from the surface to the interior of the solidified specimen as a function of reaction times are shown in Fig. 5. The oxygen and yttrium contents were greater on the surface than inside the specimen. The oxygen and yttrium contents decreased rapidly from the surface towards the interior of the specimen. Hence, a reaction layer existed between the mould and the melt. According to Fig. 5, an Al-segregation region was not formed at the surface of the specimen, which is different from the results reported by Cui⁵⁰. This difference arises from the specimen being melted and directionally solidified in the Al_2O_3 crucible with the Y_2O_3 skull under controlled solidification parameters, specifically, the temperature gradient and the growth rate. The cooling rate at the surface of the specimen was lower, and the composition did not affect the solidification path.

The reactivity of the mould and the TiAl melt is related to the Gibbs free energy changes during the reaction. Kostov⁵¹ recently reported that the standard Gibbs free energy of Y_2O_3 is more negative than that of Ti oxides (i. e., TiO, Ti_2O_3 , TiO_2). Thus, the molten TiAl alloy does not react with the Y_2O_3 skull spontaneously. However, a reaction layer is formed in the directionally solidified specimen. Saha *et al.*^{52,53} have indicated that the standard Gibbs free energy could not fully explain the reactivity of the oxides and the molten metal. According to previous research results^{30,50} the increased oxygen in the specimen during solidification is dependent on the dissolution of the Y_2O_3 according to the following reaction:



On the basis of the data presented in Fig. 5, the thickness of the surface layer increased with increasing growth distance or, more specifically, with increasing reaction time between the Y_2O_3 layer and the melt. Kuang⁴⁷ reported that the relationship between the width of the reaction layer and the reaction time can be represented as follows:

$$W = C \cdot t^n \quad (2)$$

where n is the time exponent and C is a constant for the given alloy and mould material. For the Ti-48Al-2Cr-2Mn (at.%) alloy, the values of n and C were 0.52 and 1.74, respectively⁴⁷. The thickness of the reaction layer increased exponentially, as a function of equation (2), with increasing reaction time.

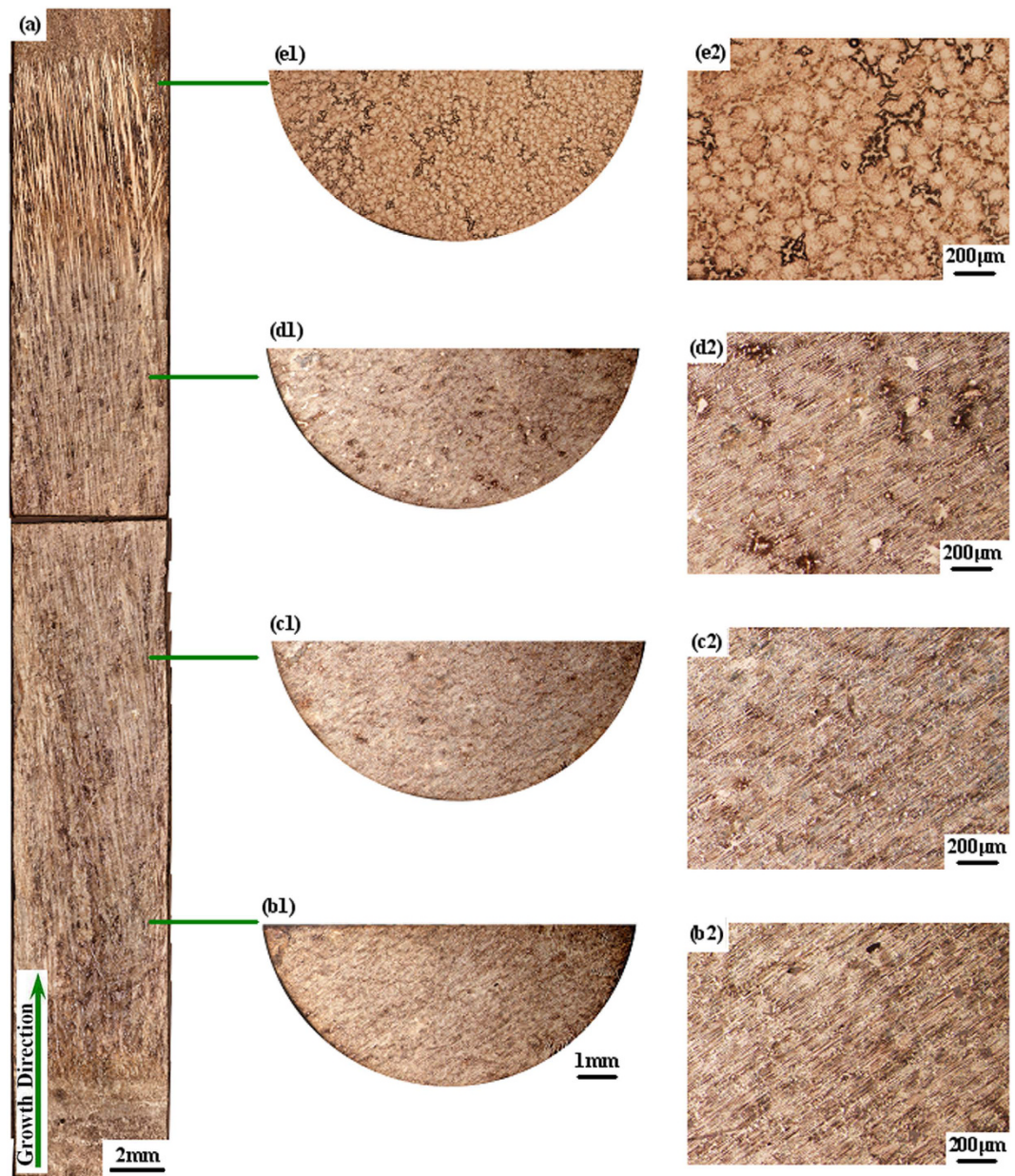


Figure 1. Microstructure of the directionally solidified Ti-43Al-3Si (at.%) at a growth rate of $10\ \mu\text{m/s}$ using Y_2O_3 skull-aided technology: (a) longitudinal section, (b) to (e) transverse sections at different distances from the bottom of the specimen at (b) 10 mm, at (c) 20 mm, at (d) 30 mm and at (e) 40 mm from the bottom of the specimen. The right sides are high magnification images corresponding to transverse sections at different positions.

To evaluate the changes in the mechanical properties from the surface to the inner core of the directionally solidified specimen, we measured the specimen's microhardness. The microhardness variation from the surface to the centre of the specimen is shown in Fig. 6. A hardened layer at the surface with a hardness of $480\text{--}510H_V$ was observed, which is greater than that of the inner core of the specimen (approximately $450H_V$). According to the observation of the surface microstructure (Fig. 4), Y_2O_3 particles did not appear in the specimen because the physical erosion of the Y_2O_3 skull was alleviated or eliminated. The greater hardness of the surface may be attributed to the solid-solute phase of oxygen that originated from the dissolution of the Y_2O_3 skull, as described by equation (1). The layer thickness increased with increasing reaction time. The thickness of this layer was less than $80\ \mu\text{m}$ for reaction times up to 5800 s (46.7 minutes). Hence, we determined the surface contamination layer was less than $80\ \mu\text{m}$ thick. This Y_2O_3 skull-aided technology is useful for the surface quality control while the casting of TiAl alloys with longer reaction times.

Variation of the oxygen content during solidification. The total oxygen content of the directionally solidified Ti-43Al-3Si (at.%) alloys increased with increasing reaction time, as shown in Fig. 7. The oxygen

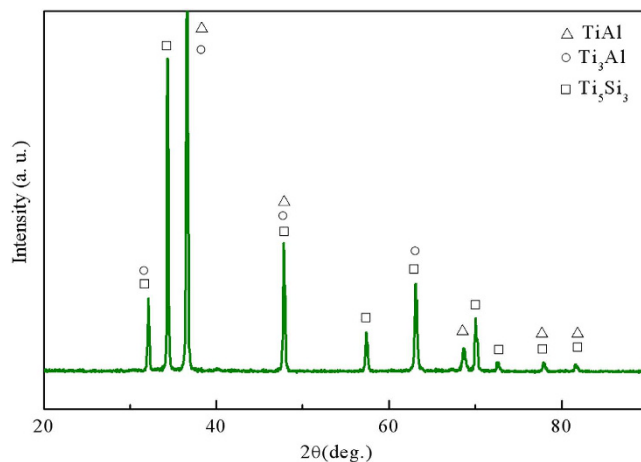


Figure 2. X-ray diffraction pattern of a directionally solidified Ti-43Al-3Si (at.%) alloy, revealing the existence of γ -TiAl, α_2 -Ti₃Al and ξ -Ti₅Si₃ phases.

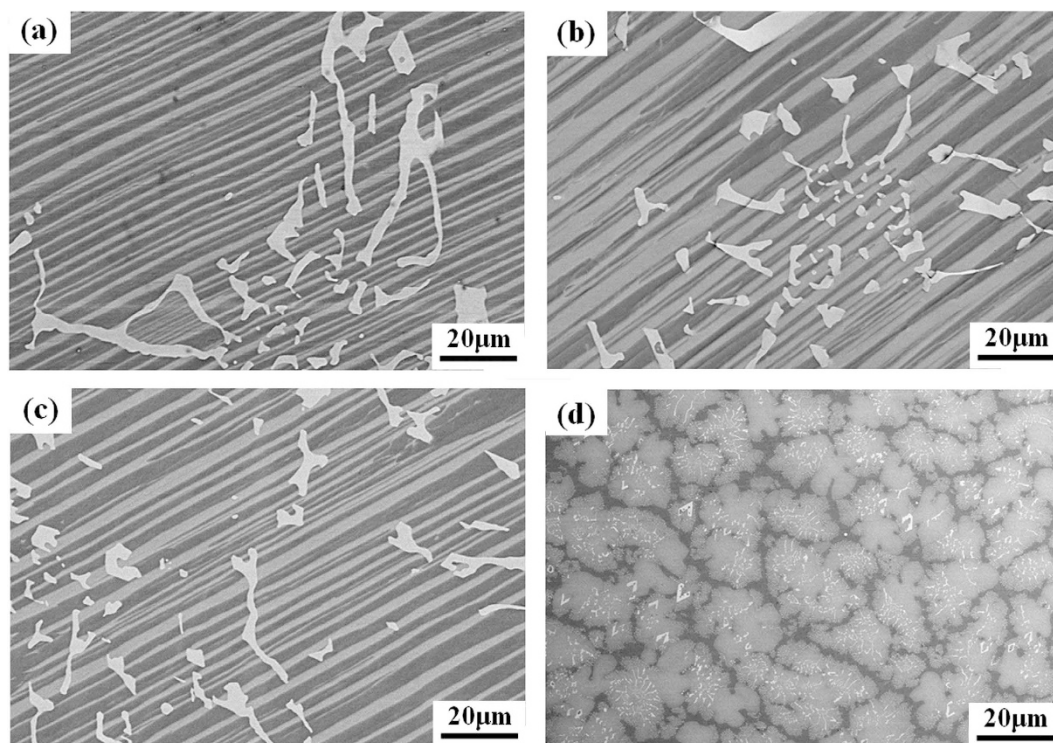


Figure 3. SEM-BSE images on transverse sections of the directionally solidified Ti-43Al-3Si (at.%) alloy with different reaction times (a) 2800 s, (b) 3800 s, (c) 4800 s and (d) 5800 s.

content of the specimen directionally solidified in the Y₂O₃ skull-aided crucible (approximately 1019–1303 ppm) was lower than that of the specimen directionally solidified in an Al₂O₃ crucible studied by Fan (approximately 2600 ppm)⁴⁹.

According to the model established by Lapin³⁰, the variation in the oxygen content with reaction time in the directionally solidified TiAl alloy can be expressed as:

$$P^3 - P_0^3 = kt \exp\left(-\frac{Q_0}{RT}\right) \quad (3)$$

where P is the oxygen content in the specimen after directional solidification, P_0 is the original oxygen content of the specimen, k is a constant, t is the reaction time, Q_0 is the activation energy, R is the universal gas constant, and T is the temperature of the melt.

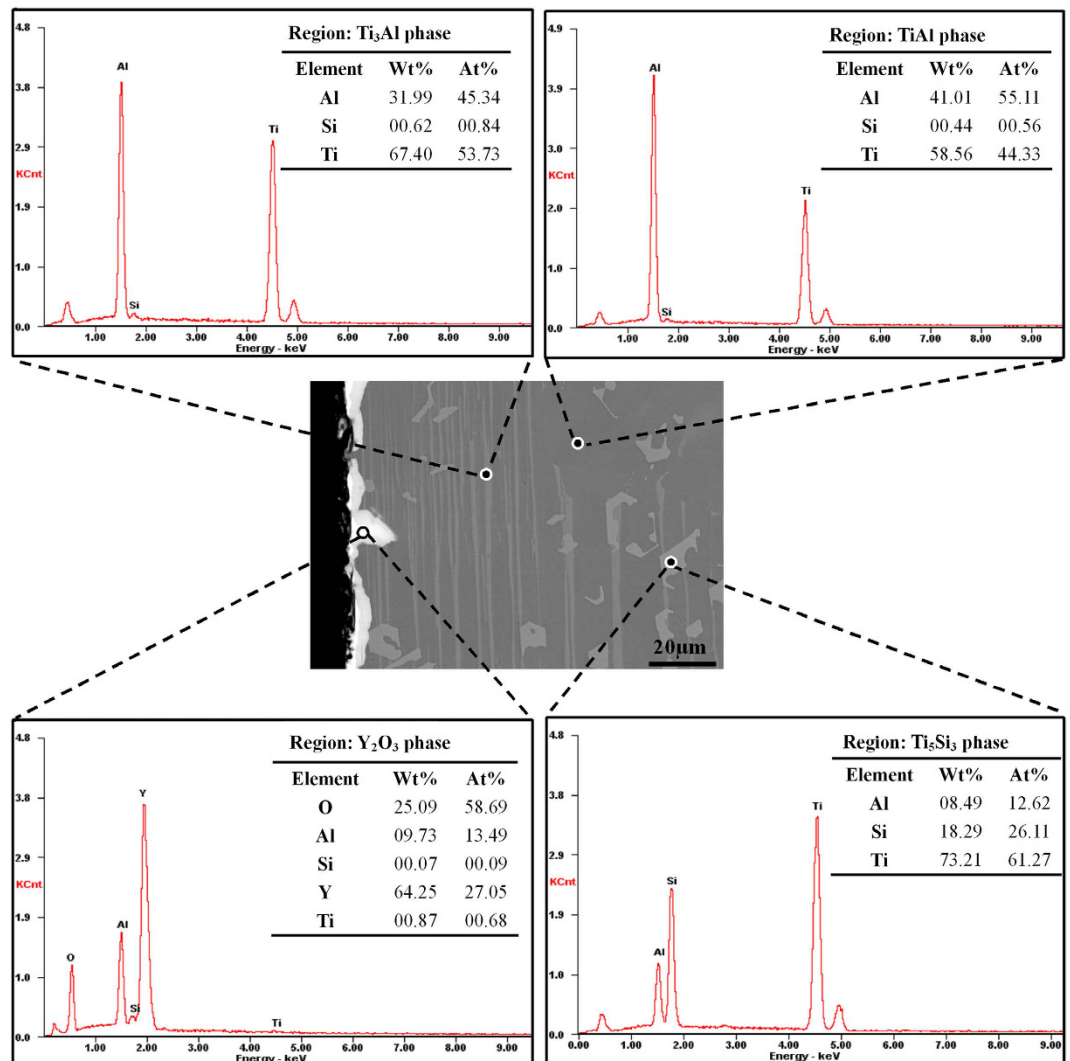


Figure 4. EDX spectrum of phases present near the surface of the Ti-43Al-3Si (at.%) specimen directionally solidified in a Y₂O₃-coated Al₂O₃ crucible.

In the current experiment, the value of P_0 (419 ppm) was smaller than P (>1000 ppm). More specifically, the value of $P_0^3 \ll P^3$. If the value of P_0 is ignored, the value of P can be simplified as

$$P = A \cdot t^{\frac{1}{3}} \quad (4)$$

where $A = [k \exp(-Q_0/RT)]^{1/3}$.

By regression analysis, the relationship between the oxygen content and the reaction time is obtained as

$$P = 1.821t^{0.345} \quad (5)$$

The regression coefficient was $R^2 = 0.9901$. The value of $t = 0.345$ agrees well with the value of $t = 1/3$ in Lapin's model³⁰.

Conclusions

- (1) A new Y₂O₃ skull-aided technology was developed to reduce the reaction between the crucible and TiAl alloy melt during the directional solidification process with longer reaction times.
- (2) After directional solidification, the specimen consisted of TiAl, Ti₃Al and Ti₅Si₃ phases. Y₂O₃ particles were not found in the specimen because the Y₂O₃ particles that split from the coating due to thermal physical erosion were markedly reduced.
- (3) The oxygen content P increased with increasing reaction time according to the equation $P = 1.821t^{0.345}$.
- (4) The hardened layer at the surface was less than 80 μm thick, which is acceptable for the surface quality control of near-net shapes and investment casting of TiAl-based alloys.

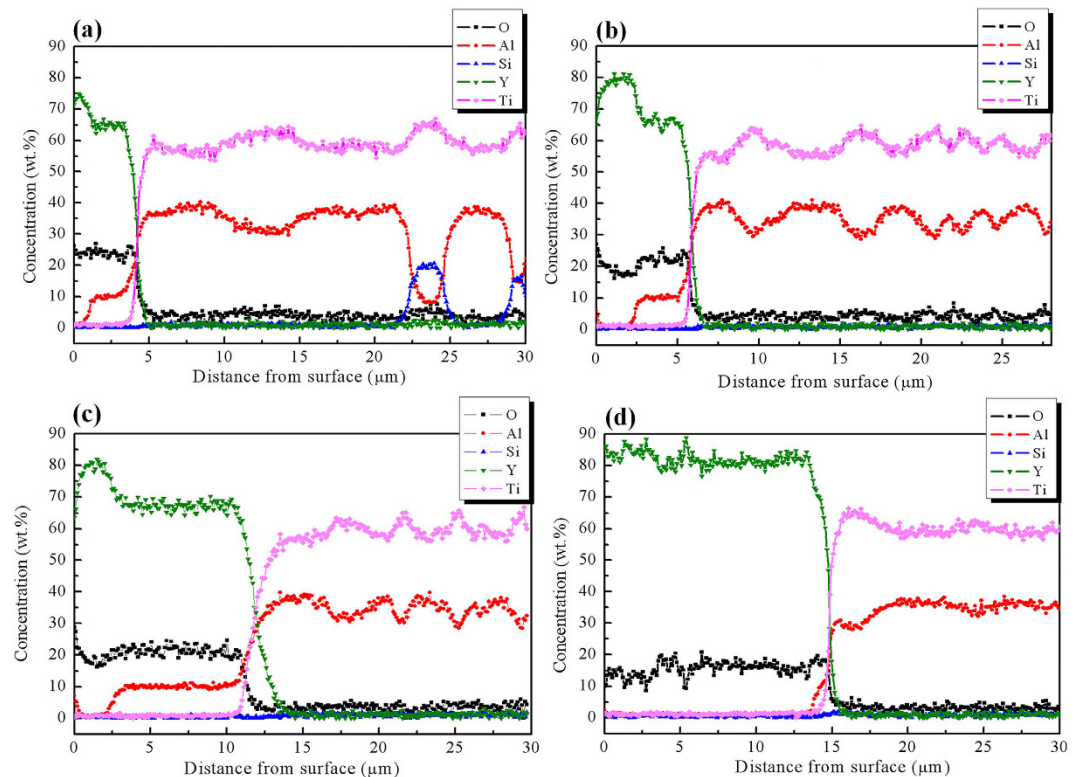


Figure 5. Elemental distribution within the depth from the surface of the directionally solidified Ti-43Al-3Si (at.%) alloys with the following reaction times: (a) 2800 s, (b) 3800 s, (c) 4800 s and (d) 5800 s.

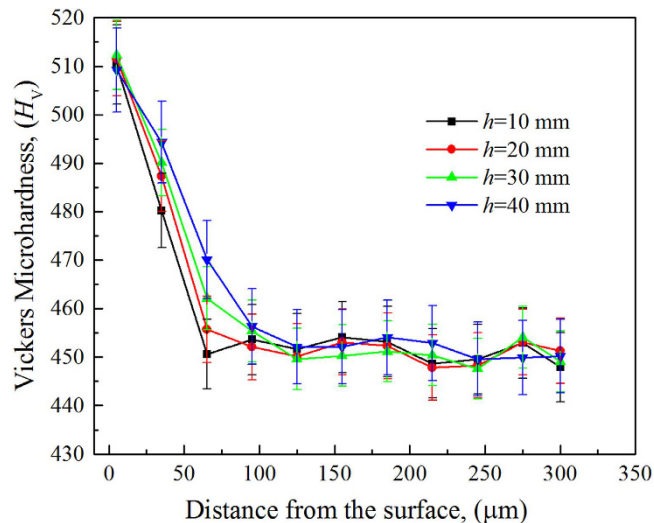


Figure 6. Microhardness profiles of the hardened layer at the surface of the Ti-43Al-3Si (at.%) alloy directionally solidified in an alumina crucible with Y_2O_3 skull-aided technology, as measured at different distances (h) from the bottom of the specimen.

Methods

The master ingot with a nominal composition of Ti-43Al-3Si (at.%) was prepared using cold crucible induction technology in an argon environment; Ti (99.7%), Al (99.9%) and Si (99.9%) were used as the raw materials. The actual chemical composition was obtained by X-ray fluorescence analysis (Axios PW 4400). The oxygen content of the alloy ingot was measured using a CHNS/O elemental analyser. The analysed samples were approximately $\varnothing 5 \text{ mm} \times 10 \text{ mm}$. The oxygen content was obtained by measuring the CO_2 present via using infrared detection. Table 1 shows the measured composition of the prepared alloy. The samples used for the directional solidification experiments were rods ($\varnothing 6 \text{ mm} \times 100 \text{ mm}$) cut from the ingot using a wire electrical discharge machine.

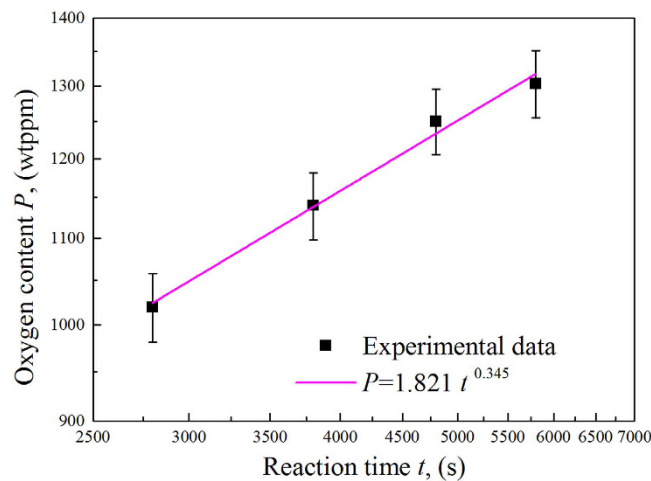


Figure 7. Variation in the oxygen content in the bulk alloy versus the reaction time for Ti-43Al-3Si (at.%) directionally solidified in an alumina crucible with Y_2O_3 skull-aided technology.

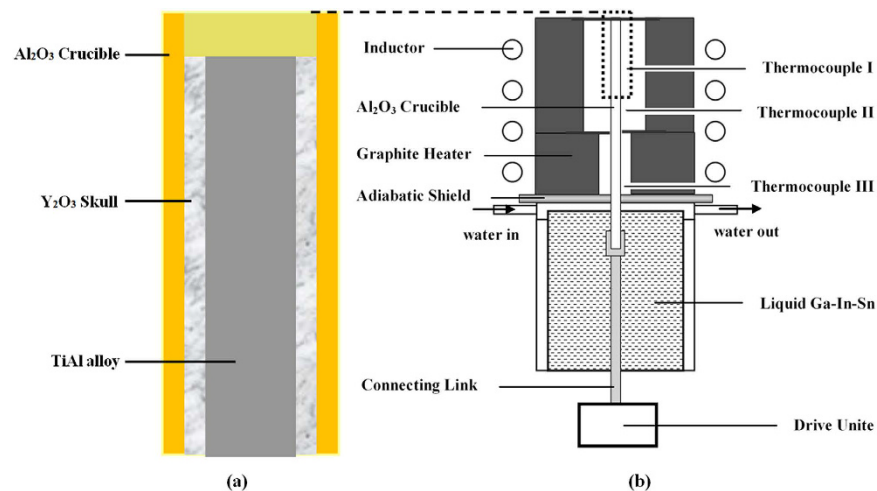


Figure 8. Schematics of (a) the specimen with skull-aided technology and (b) the Bridgman-type directional solidification furnace.

To minimize the reaction between the Al_2O_3 crucible and the melt, a skull-aided technology was used for the directional solidification of the TiAl-based alloy. This technology used fine mixed powders (nanoscale and microscale) of high-purity Y_2O_3 without a binder to fill in the interspaces between the alumina crucible and the specimen under a certain pressure. A schematic of the technology is shown in Fig. 8a. The pressure and density of the Y_2O_3 skull were carefully controlled. After the specimen and crucible were heated, the Y_2O_3 coat became an integral skull and separated the melt from the Al_2O_3 crucible.

The directional solidification experiments were performed in a Bridgman-type system, as shown in Fig. 8b. The samples were placed into 99.99% pure alumina crucibles with a 6.5/7.5 mm diameter (inside/outside diameter) Y_2O_3 skull and a length of 100 mm. Because of the reactivity of the molten TiAl alloy, the temperature gradient was measured by W/Re thermocouples that were positioned near the outside surface of the alumina tubes to avoid damaging the thermocouple, as shown in Fig. 8b. The chamber of the directional solidification furnace was evacuated to 10^{-4} Pa and filled with argon to avoid oxidation. The specimen was heated to 1823 K over 2 h and thermally stabilized for 1800 s. The specimen was then directionally solidified with a growth rate of $10 \mu\text{m/s}$. The growth length of the samples was 40 mm during the directional solidification process. At the end of the experiment, the sample was quenched with a liquid Ga-In-Sn alloy to restore the solid/liquid interface.

The reaction time t_2 during directional solidification was calculated by d/V , where d is the growth distance and V is growth rate. Because the time needed to thermally stabilize the specimen was $t_1 = 1800$ s, the total reaction time t was $t = t_1 + t_2$.

The specimens were cut, polished and etched with a solution of 10 mL HF, 10 mL of HNO_3 , and 180 mL of H_2O for further analysis. Both optical microscopy (OM) and SEM with the BSE mode were used to characterize the microstructure of the specimens. The phases were identified using a Rigaku D/max-RB X-ray diffractometer

Element	Ti	Al	Si	O
at.%	Balance	43.27	3.08	0.10 (419 ppm)

Table 1. Chemical composition of the Ti-43Al-3Si (at.%) ingot.

equipped with a monochromatic Cu-K α radiation source. The elemental distributions were analysed by electron probe microanalysis (EPMA) under an acceleration voltage of 15 kV ($\pm 2\%$ to 5%).

To evaluate the thickness of the hardened layer, the microhardness values were measured on transverse sections of the specimens with a test load of 100 g, and a dwell time of 10 s. The adopted values of the microhardness were the average values of at least 10 tests on each sample.

References

- Su, Y. *et al.* Lamellar Orientation Control in Directionally Solidified TiAl Intermetallics. *China Foundry* 219–231 (2014).
- Clemens, H. & Mayer, S. Design, Processing, Microstructure, Properties, and Applications of Advanced Intermetallic TiAl Alloys. *Adv. Eng. Mater.* **15**, 191–215 (2013).
- Wu, X. Review of Alloy and Process Development of TiAl Alloys. *Intermetallics*. **14**, 1114–1122 (2006).
- Clemens, H. & Kestler, H. Processing and Applications of Intermetallic γ -TiAl-based Alloys. *Adv. Eng. Mater.* **2**, 551–570 (2000).
- Loria, E. A. Gamma Titanium Aluminides as Prospective Structural Materials. *Intermetallics*. **8**, 1339–1345 (2000).
- Gupta, R. K., Pant, B. & Sinha, P. P. Theory and Practice of $\gamma+\alpha_2$ Ti Aluminide: A Review. *Trans. Indian Ins. Met.* **67**, 143–165 (2014).
- Fu, P. X. *et al.* Centrifugal Casting of TiAl Exhaust Valves. *Intermetallics*. **16**, 130–138 (2008).
- Johnson, D. R., Chihara, K., Inui, H. & Yamaguchi, M. Microstructural Control of TiAl-Mo-B Alloys by Directional Solidification. *Acta Mater.* **46**, 6529–6540 (1998).
- Johnson, D. R., Masuda, Y., Inui, H. & Yamaguchi, M. Alignment of the TiAl/Ti₃Al Lamellar Microstructure in TiAl Alloys by Growth From a Seed Material. *Acta Mater.* **45**, 2523–2533 (1997).
- Liu, G. *et al.* Study On the Microstructure, Phase Transition and Hardness for the TiAl–Nb Alloy Design During Directional Solidification. *J. Alloys Compd.* **650**, 45–52 (2015).
- Kartavykh, A. V., Tcherdyntsev, V. V., Gorshenkov, M. V. & Kaloshkin, S. D. Microstructure Engineering of TiAl-based Refractory Intermetallics within Power-Down Directional Solidification Process. *J. Alloys Compd.* **586**, Supplement 1, S180–S183 (2014).
- Ding, X. F., Lin, J. P., Zhang, L. Q., Su, Y. Q. & Chen, G. L. Microstructural Control of TiAl–Nb Alloys by Directional Solidification. *Acta Mater.* **60**, 498–506 (2012).
- Fan, J. *et al.* Lamellar Orientation Control of Directionally Solidified Ti-46Al-0.5W-0.5Si Alloy by Self-Seeding Technology. *Mater. Sci. Tech.* **30**, 183–188 (2014).
- Lapin, J. & Gabalcová, Z. Solidification Behavior of TiAl-based Alloys Studied by Directional Solidification Technique. *Intermetallics*. **19**, 797–904 (2011).
- Chen, R. *et al.* A Novel Method for Grain Refinement and Microstructure Modification in TiAl Alloy by Ultrasonic Vibration. *Mater. Sci. Eng. A*. **653**, 23–26 (2016).
- Dong, S. *et al.* Deformation Behavior and Microstructural Evolution of Directionally Solidified TiAlNb-based Alloy During Thermo-Compression at 1373–1573K. *Mater. Des.* **84**, 118–132 (2015).
- Chen, R. *et al.* Microstructure Evolution and Mechanical Properties of Directionally-Solidified TiAlNb Alloy in Different Temperature Gradients. *J. Alloys Compd.* **648**, 667–675 (2015).
- Dong, S. *et al.* Microstructure Control and Mechanical Properties of Ti44Al6Nb1.0Cr2.0V Alloy by Cold Crucible Directional Solidification. *Mater. Sci. Eng. A*. **614**, 67–74 (2014).
- Ding, H., Wang, Y., Chen, R., Guo, J. & Fu, H. Effect of Growth Rate On Microstructure and Tensile Properties of Ti–45Al–2Cr–2Nb Prepared by Electromagnetic Cold Crucible Directional Solidification. *Mater. Des.* **86**, 670–678 (2015).
- Du, Y., Shen, J., Xiong, Y., Ren, C. & Fu, H. Lamellar Microstructure Alignment in Ti-47Al Alloy by Electromagnetic Confinement and Directional Solidification Using a Seed. *Jom-Us*. **67**, 1258–1264 (2015).
- Du, Y. *et al.* Determining the Effects of Growth Velocity on Microstructure and Mechanical Properties of Ti-47Al Alloy using Electromagnetic Confinement and Directional Solidification. *Jom-Us*. **66**, 1914–1922 (2014).
- Du, Y. *et al.* Lamellar Microstructure Alignment and Fracture Toughness in Ti–47Al Alloy by Electromagnetic Confinement and Directional Solidification. *Mater. Sci. Eng. A*. **621**, 94–99 (2015).
- Tetsui, T., Kobayashi, T., Kishimoto, A. & Harada, H. Structural Optimization of an Yttria Crucible for Melting TiAl Alloy. *Intermetallics*. **20**, 16–23 (2012).
- Lapin, J., Gabalcová, Z. & Pelachová, T. Effect of Y₂O₃ Crucible On Contamination of Directionally Solidified Intermetallic Ti–46Al–8Nb Alloy. *Intermetallics*. **19**, 396–403 (2011).
- Kuang, J. P., Harding, R. A. & Campbell, J. Investigation Into Refractories as Crucible and Mould Materials for Melting and Casting γ -TiAl Alloys. *Mater. Sci. Tech.* **16**, 1007–1016 (2000).
- Frueh, C., Poirier, D. R., Maguire, M. C. & Harding, R. A. Attempts to Develop a Ceramic Mould for Titanium Casting—A Review. *Int. J. Cast. Metal. Res.* **9**, 233–239 (1996).
- Bewlay, B. P., Nag, S., Suzuki, A. & Weimer, M. J. TiAl Alloys in Commercial Aircraft Engines. *Mater. High Temp.* (2016).
- Clemens, H. & Mayer, S. Intermetallic Titanium Aluminides in Aerospace Applications – Processing, Microstructure and Properties. *Mater. High Temp.* **33**, 560–570 (2016).
- Cui, R. *et al.* Interactions Between γ -TiAl Melt and Y₂O₃ Ceramic Material During Directional Solidification Process. *Trans. Nonferrous Met. Soc. China*. **21**, 2415–2420 (2011).
- Lapin, J. & Gabalcová, Z. Solidification Behaviour of TiAl-based Alloys Studied by Directional Solidification Technique. *Intermetallics*. **19**, 797–804 (2011).
- Gomes, F., Barbosa, J. & Ribeiro, C. S. Induction Melting of γ -TiAl in CaO Crucibles. *Intermetallics*. **16**, 1292–1297 (2008).
- Fan, J., Li, X., Su, Y., Guo, J. & Fu, H. Dependency of Microhardness On Solidification Processing Parameters and Microstructure Characteristics in the Directionally Solidified Ti–46Al–0.5W–0.5Si Alloy. *J. Alloys Compd.* **504**, 60–64 (2010).
- Lapin, J., Ondrůš, L. & Nazmy, M. Directional Solidification of Intermetallic Ti-46Al-2W-0.5Si Alloy in Alumina Moulds. *Intermetallics*. **10**, 1019–1031 (2002).
- Fan, J., Li, X., Su, Y., Guo, J. & Fu, H. The Microstructure Parameters and Microhardness of Directionally Solidified Ti–43Al–3Si Alloy. *J. Alloys Compd.* **506**, 593–599 (2010).
- Fan, J. *et al.* Microstructure Evolution and Interfacial Reaction of TiAl–Si Alloy Solidified in Alumina Crucible. *Mater. Sci. Tech.* **31**, 1727–1734 (2015).
- Lapin, J., Ondrůš, L. & Bajana, O. Effect of Al₂O₃ Particles On Mechanical Properties of Directionally Solidified Intermetallic Ti-46Al-2W-0.5Si Alloy. *Mater. Sci. Eng. A*. **360**, 85–95 (2003).

37. Cheng, X., Yuan, C., Blackburn, S. & Withey, P. A. The Influence of ZrO₂ Concentration in an Yttria-Based Face Coat for Investment Casting a Ti-45Al-2Mn-2Nb-0.2TiB Alloy Using a Sessile Drop Method. *Metall. Mater. Trans. A*, **46**, 1328–1336 (2015).
38. Jia, Q., Cui, Y. Y. & Yang, R. Intensified Interfacial Reactions Between Gamma Titanium Aluminide and CaO Stabilised ZrO₂. *Int. J. Cast. Metal. Res.* **17**, 23–28 (2004).
39. Yuan, C., Cheng, X. & Withey, P. A. Investigation Into the Use of CaZrO₃ as a Facecoat Material in the Investment Casting of TiAl Alloys. *Mater. Chem. Phys.* **155**, 205–210 (2015).
40. Kartavykh, A. V., Tcherdyntsev, V. V. & Zollinger, J. TiAl–Nb Melt Interaction with AlN Refractory Crucibles. *Mater. Chem. Phys.* **116**, 300–304 (2009).
41. Kartavykh, A. V., Tcherdyntsev, V. V. & Zollinger, J. TiAl–Nb Melt Interaction with Pyrolytic Boron Nitride Crucibles. *Mater. Chem. Phys.* **119**, 347–350 (2010).
42. Gao, M. *et al.* Physical Erosion of Yttria Crucibles in Ti–54Al Alloy Casting Process. *J. Mater. Process. Tech.* **211**, 2004–2011 (2011).
43. Kartavykh, A. V. *et al.* A Promising Microstructure/Deformability Adjustment of B-Stabilized γ -TiAl Intermetallics. *Mater. Lett.* **162**, 180–184 (2016).
44. Yamaguchi, M., Johnson, D. R., Lee, H. N. & Inui, H. Directional Solidification of TiAl-based Alloys. *Intermetallics*, **8**, 511–517 (2000).
45. Johnson, D. R., Inui, H. & Yamaguchi, M. Crystal Growth of TiAl Alloys. *Intermetallics*, **6**, 647–652 (1998).
46. Du, Y., Shen, J., Xiong, Y., Shang, Z. & Fu, H. Stability of Lamellar Microstructures in a Ti–48Al–2Nb–2Cr Alloy During Heat Treatment and its Application to Lamellae Alignment as a Quasi-Seed. *Intermetallics*, **61**, 80–84 (2015).
47. Kuang, J. P., Harding, R. A. & Campbell, J. A Study of Refractories as Crucible and Mould Materials for Melting and Casting gamma-TiAl Alloys. *Int. J. Cast. Metal. Res.* **13**, 277–292 (2001).
48. Cheng, X., Yuan, C., Shevchenko, D. & Withey, P. The Influence of Mould Pre-Heat Temperature and Casting Size On the Interaction Between a Ti–46Al–8Nb–1B Alloy and the Mould Comprising an Al₂O₃ Face Coat. *Mater. Chem. Phys.* **146**, 295–302 (2014).
49. Fan, J., Li, X., Su, Y., Guo, J. & Fu, H. Effect of Growth Rate On Microstructure Parameters and Microhardness in Directionally Solidified Ti–49Al Alloy. *Mater. Des.* **34**, 552–558 (2012).
50. Cui, R., Cao, M., Zhang, H. & Gong, S. Interactions Between TiAl Alloys and Yttria Refractory Material in Casting Process. *J. Mater. Process. Tech.* **210**, 1190–1196 (2010).
51. Kostov, B. & Friedrich, A. Selection of Crucible Oxides in Molten Titanium and Titanium Aluminum Alloys by Thermo-Chemistry Calculations. *J. Min. Met.* **41B**, 113–125 (2005).
52. Saha, R. L., Nandy, T. K., Misra, R. & Jacob, K. T. Evaluation of the Reactivity of Titanium with Mould Materials During Casting. *Bull. Mater. Sci.* (1999).
53. Saha, R. L., Nandy, T. K., Misra, R. D. K. & Jacob, K. T. On the Evaluation of Stability of Rare Earth Oxides as Face Coats for Investment Casting of Titanium. *Metal. Trans. B*, **21**, 559–566 (1990).

Acknowledgements

The authors are grateful for the financial support of the National Natural Science Foundation of China (Grants no. 51501167), the Science and Technology Open Cooperation Project of Henan Province (Grant no. 162106000019) and the Doctor Research Foundation of Zhengzhou University of Light Industry (Grant no. 2014BSJJ049).

Author Contributions

J.L.F., J.X.L. and J.J.G. designed the experiments. S.W. and S.Y.W. carried out the experiments. S.X.T. analysed the microstructures and performed the hardness tests. X.W. performed the oxygen content tests. J.L.F., X.W. and J.J.G. wrote the paper. All authors discussed the results and commented on the manuscript.

Additional Information

Competing Interests: The authors declare no competing financial interests.

How to cite this article: Fan, J. *et al.* Microstructure formation and interface characteristics of directionally solidified TiAl–Si alloys in alumina crucibles with a new Y₂O₃ skull-aided technology. *Sci. Rep.* **7**, 45198; doi: 10.1038/srep45198 (2017).

Publisher's note: Springer Nature remains neutral with regard to jurisdictional claims in published maps and institutional affiliations.



This work is licensed under a Creative Commons Attribution 4.0 International License. The images or other third party material in this article are included in the article's Creative Commons license, unless indicated otherwise in the credit line; if the material is not included under the Creative Commons license, users will need to obtain permission from the license holder to reproduce the material. To view a copy of this license, visit <http://creativecommons.org/licenses/by/4.0/>

© The Author(s) 2017